ARTICLES

Molecular Assembly Structure of CCl_4 in Graphitic Nanospaces

T. Iiyama,[†] K. Nishikawa,[‡] T. Suzuki,[§] T. Otowa,[||] M. Hijiriyama,[||] Y. Nojima,[||] and K. Kaneko*,[†]

Physical Chemistry, Material Science, Graduate School of Science and Technology, Chiba University, Phase Science, Diversity and Fractal Science, Graduate School of Science and Technology, Chiba University, Department of Chemistry, Faculty of Science, Chiba University 1-33 Yayoi, Inage, Chiba 263, Japan, and Research and Development Center, The Kansai Coke and Chemicals Co. Ltd., 1-1 Ohama, Amagasaki, Hyogo 660, Japan

Received: August 8, 1996[⊗]

The X-ray diffraction of CCl_4 molecules adsorbed in slit-shaped graphitic micropores was measured at 303 K. The effect of the pore width in the range of 0.75−1.13 nm on the structure of CCl_4 molecular assembly in the micropores was examined. The electron radial distribution function (ERDF) analysis was applied to the diffraction data, and the ERDFs from only adsorbed molecular assembly were determined. The peak position of ERDF due to the first-nearest-neighbor coordination agreed with that of the bulk liquid, but other peaks shifted from those of the bulk liquid. The second-nearest-neighbor peak shifted to a smaller side, indicating the presence of a more dense short range structure of the molecular assembly in the micropore. The peak intensities were noticeably weaker than those of the bulk liquid, and the tendency became significant with the decrease of the pore width. These behaviors indicate a serious restriction for the molecular assembly structure in the narrow micropore. Although the bulk liquid has a clear regular coordination structure up to the fourth-nearest-neighbor range, the structure of molecular assembly in the micropores smears around the third or fourth neighbors.

Introduction

The surface−admolecular interaction is remarkably enhanced by the overlapping of interactions from opposite pore walls in a micropore whose pore width is less than 2 nm.[1,2] As molecules are adsorbed by the strong molecule−pore interaction, admolecules are densely packed in the micropore, and thereby not only the surface−molecule interaction but also the intermolecular interaction is noticeably enhanced.[3,4] The enhanced intermolecular interaction should affect the structure and behavior of molecules adsorbed in the micropore. Recent studies suggested the formation of the unusual molecular assembly structures, such as dimer formation of NO,[5,6] the magnetic cluster formation of O_2,[7] the dipole-oriented structure of SO_2,[8] and the molecular clathrate formation of NO and H_2O.[9] The solid NMR approach also indicated the presence of the special molecular state of N_2 in the micropore.[10] However a direct structure determination of the molecular assembly has been requested with the use of X-ray diffraction.

Microporous carbon has gathered much attention from the fundamental and practical aspects.[11−17] In particular activated carbon fibers (ACFs) and superhigh surface area carbons (HSACs) have quite uniform micropores of great capacity compared with conventional activated carbons.[18−20] The micropore walls are mainly composed of micrographitic crystallites, and the micropores are of slit shape.[18,21] Consequently ACFs or HSACs can offer the slit-shaped graphitic micropores. As the graphitic micropores provide reliable experimental data for the theoretical studies,[22−24] the structural experiment on the molecular assembly in the graphitic micropores has been strongly desired. Furthermore such a structural study on the molecules adsorbed in the micropores should shed light on the density of the adsorbed phase, which accelerates an essential progress in adsorption science and technology. X-rays can penetrate these carbon materials, and X-ray diffraction technique can be applied to the structural study of the molecular assembly in the micropores of ACF or HSAC.

The authors showed the effectiveness of the X-ray diffraction method for the molecular assembly of H_2O in the graphitic micropore in the preceding letter.[25] In the letter we showed the presence of the well-organized structure of H_2O, but we need an established analytical method for the X-ray diffraction data to get more quantitative information on molecular assembly. We selected CCl_4 molecules for this purpose. A CCl_4 molecule is completely neutral, and the molecular geometry can be approximated by a spherical shape.

CCl_4 has following merits as an adsorbate for this research. The liquid structure of CCl_4 was studied by several authors.[26−28] Nishikawa and Murata reported that the liquid CCl_4 has a long range correlation over 2 nm at room temperature.[28] The structure of liquid CCl_4 was investigated by the structure simulation.[29] Thus, we can compare the data on the adsorbed molecules with those of bulk liquid. The molecular diameter of CCl_4 is 0.59 nm, and the structure of molecules adsorbed in micropores is expected to be sensitive to the micropore width. A CCl_4 molecule has a large X-ray scattering ability compared

[†] Physical Chemistry, Material Science, Chiba University.
[‡] Phase Science, Diversity and Fractal Science, Chiba University.
[§] Department of Chemistry, Faculty of Science, Chiba University.
[||] The Kansai Coke and Chemicals Co. Ltd.
[⊗] Abstract published in *Advance ACS Abstracts,* April 1, 1997.

S1089-5647(96)02408-X CCC: $14.00

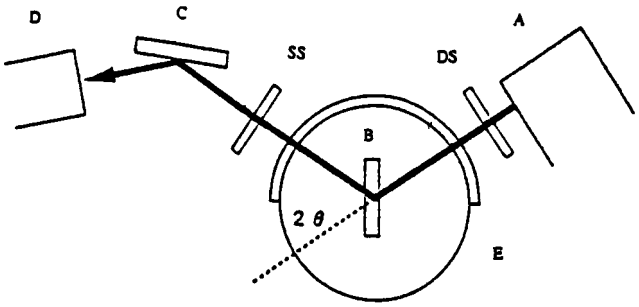

Figure 1. Schematic diagram of experimental arrangement. A, X-ray tube; B, sample; C, graphite monochrometer; D, scintillation counter; E, sample chamber (the details are shown in Figure 2); DS, dispersion slit (1.0°); SS, scattering slit (1.0°).

with the carbon atom of the solid system. The X-ray self-scattering factor I_{self} at $s = 0$ (s, scattering parameter; $s = (4\pi \sin \theta)/\lambda$; 2θ is the scattering angle, λ is the wavelength of the X-ray), which plays a role in the criterion for X-ray scattering ability, is given by

$$I_{self}(0) = \sum_i Z_i^2 \tag{1}$$

Here Z_i is the electron number of a component atom i. The X-ray self-scattering factors at $s = 0$ for a CCl_4 molecule and a carbon atom, $I_{self}^{CCl_4}(0)$ and $f_{self}^{C}(0)$, are 1192 and 36, respectively. Therefore, we can approximate that the X-ray diffraction intensity of only adsorbed CCl_4 is obtained. In addition to the above reasons, CCl_4 is a model compound of halocarbons as pollutants, and information on CCl_4 adsorbed in the carbon micropore is quite important from the environmental viewpoint.

In this paper, an analytical approach to the X-ray diffraction data on the intermolecular structure of CCl_4 molecules adsorbed in the carbon micropore and the intermolecular structures of CCl_4 in the micropore at 303 K are described.

Experimental Section

Three kinds of pitch-based activated carbon fibers (ACFs) (P-5, P-10, and P-20) were used as adsorbents. Three ACF samples have different porosities. The micropore structures were determined by N_2 adsorption at 77 K, and they were already published in the previous article.[4] The CCl_4 adsorption isotherm was gravimetrically determined at 303 K after preheating at 383 K and 1 mPa for 2 h.

The experimental arrangement of the X-ray diffraction is shown in Figure 1. The intensity from CCl_4 adsorbed in the micropore at 303 K was measured with the transmission method by use of an angle-dispersion diffractometer (MXP3 system, MAC Science). The X-ray tube, counter, and monochrometer can rotate in the vertical plane around the goniometer center, which has the $\theta-2\theta$ system, while sample holder was fixed. The X-ray tube was operated at 50 kV and 35 mA. The monochromatic X-ray from Mo Kα radiation was used for the diffraction measurement, and the observable range of the scattering parameter s was from 7 to 120 nm^{-1}. Figure 2 shows the in situ X-ray diffraction chamber of 96 mm in diameter. The sample holder (Figure 2B) is installed in the chamber (Figure 2A). Mylar films were used for the windows of the in situ measuring chamber and the sample holder. The sample chamber was connected to the adsorption system in order to control the atmosphere of ACF samples. As the sample holder is open, CCl_4 molecules are adsorbed on ACF samples in the holder.

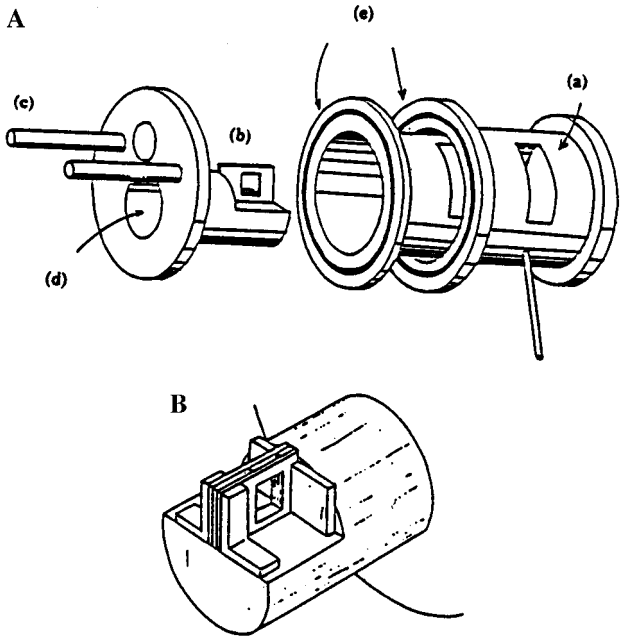

Figure 2. (A) Schematic illustration of the sample chamber. a, Mylar film as an X-ray window; b, sample holder (1 mm thickness); c, stainless pipe to the vacuum line; d, heater and heat sink; e, O-ring. (B) Sample holder.

Analysis Method of X-ray Diffraction Data

Intensity Correction. The observed X-ray scattering intensity at s, $I_{obs}(s)$, of the carbon sample having adsorbed CCl_4 is given by

$$I_{obs}(s) = I_{tot}(s)\cdot P(\theta)\cdot G(\theta)\cdot A(\theta,p) + I_{back}(s)\cdot A(\theta,p) \tag{2}$$

Here $I_{tot}(s)$ is the X-ray scattering intensity of the sample at s. The polarization factor, $P(\theta)$, is given by

$$P(\theta) = \frac{1 + \cos^2 2\alpha\cdot\cos^2 2\theta}{1 + \cos^2 2\alpha} \tag{3}$$

Here 2α is the scattering angle on the monochrometer. The geometrical factor, $G(\theta)$, for a normalization of X-ray irradiating volume is simply given by

$$G(\theta) = \frac{1}{\cos \theta} \tag{4}$$

The notation $I_{back}(s)$ is the parasitic scattering that is mainly attributed to the scattering by the windows of the sample cell. It can be determined experimentally by the measurement of the sample cell without sample in vacuo. The X-ray absorption factor, $A(\theta,p)$, depends on both the scattering angle 2θ and extent of CCl_4 adsorption. It is given by

$$A(\theta,p) = \exp\{-\mu_s(p)\cdot l_s/\cos \theta - \mu_g(p)\cdot l_g\} \tag{5}$$

where $\mu_s(p)$ and $\mu_g(p)$ are the linear X-ray absorption coefficients of the sample and the gas phase, which depend on the CCl_4 absolute pressure, p, and l_s and l_g are the X-ray path length of the sample and X-ray path length of the gas phase, respectively. The first term in the exponent of eq 5 expresses the X-ray absorption by the carbon sample and adsorbed CCl_4 molecules, and the second term stems from absorption by gaseous CCl_4 in the sample chamber. The first term is much greater than the second one under these experimental conditions. Further, $\mu_s(p)\cdot l_s$ can be expressed by

$$\mu_s(p)\cdot l_s = \log\frac{I_a}{I_0} - \mu_g(p)\cdot l_g \quad (6)$$

Here I_a is the transmitting X-ray intensity with the sample and I_0 is that without the sample at $\theta = 0°$. Both I_a and I_0 were measured at 20 kV and 10 mA using an aluminum plate 2 mm in thickness as the X-ray attenuator in this work. The notation of μ_g is calculated with the following equation.

$$\mu_g(p) = \left(\frac{\mu}{\rho}\right)_{CCl_4}\cdot\frac{pM}{RT} \quad (7)$$

Here, $(\mu/\rho)_{CCl_4}$ is the mass X-ray absorption coefficient that is calculated from the literature values,[30] and M is the molecular weight of CCl_4, R and T are the gas constant and the measuring absolute temperature. The value of l_g is determined by the sample chamber geometry ($l_g = 96$ mm in this experiment).

Extraction Procedure of Scattering Intensity from an Adsorbed CCl_4 Assembly. The scattering intensity from only adsorbed CCl_4 assembly must be extracted from the observed X-ray scattering intensity $I_{tot}(s)$. We assume the additive form of scatterings by carbon wall ($I^C_{tot}(s)$) and by adsorbed molecules ($I^{CCl_4}_{tot}(s)$), and the interference term due to adsorbed molecules and carbon walls ($I_{int}(s)$), as described by

$$I_{tot}(s) = I^C_{tot}(s) + I^{CCl_4}_{tot}(s) + I_{int}(s) \quad (8)$$

Although water adsorption affects the micrographitic structure of ACFs,[31] it is expected that CCl_4 adsorption does not change the structure. In the present case, the first term, $I^C_{tot}(s)$, can be obtained experimentally from the diffraction data of the carbon only, $I^C_{obs}(s)$, without adsorption of CCl_4.

$$I^C_{obs}(s) = I^C_{tot}(s)\cdot P(\theta)\cdot G(\theta)\cdot A(\theta,p=0) + I_{back}(s)\cdot A(\theta,p=0) \quad (9)$$

These correcting factors, $P(\theta)$, $G(\theta)$, $A(\theta,p)$, and $I_{back}(s)$, were described above. The interference term is given by

$$I_{int}(s) = \sum_{j,k}^{j\neq k} f_C\, f_{CCl_4}\frac{\sin sr_{jk}}{sr_{jk}} \quad (10)$$

Here, f_{CCl_4} is the CCl_4 molecular scattering factor, which is approximated by

$$f_{CCl_4} = \sqrt{f_C^2 + 4f_{Cl}^2} \quad (11)$$

where f_C and f_{Cl} are atomic scattering factors of carbon and chlorine atoms, respectively. The notation r_{jk} in eq 10 is the distance between the jth carbon atom and the kth adsorbed CCl_4 molecule. The third term of eq 8 is smaller than the second term, which is approximately proportional to f_{CCl_4}. Therefore, $I^{CCl_4}_{tot}(s)$, the scattering intensity of the adsorbed CCl_4, can be determined as

$$I^{CCl_4}_{tot}(s) = I_{tot}(s) - I^C_{tot}(s) \quad (12)$$

Electron Radial Distribution Function Analysis. The X-ray diffraction of the adsorbed CCl_4 molecular assembly, $I^{CCl_4}_{tot}(s)$, consists of coherent and incoherent X-ray scatterings, as given by eq 13.

$$I^{CCl_4}_{tot}(s) = I_e\{I^{CCl_4}_{coh}(s) + \Phi(s)\cdot I^{CCl_4}_{inc}(s)\} \quad (13)$$

The incoherent scattering, $I^{CCl_4}_{inc}(s)$, was removed by using of literature values.[30] $\Phi(s)$ is the function that depends on the experimental condition of the monochrometer. The coherent scattering, $I^{CCl_4}_{coh}(s)$, was fitted to the self-scattering factor[30] at large s regions to determine the normalization factor, I_e

$$I^{CCl_4}_{coh}(s_{max}) \approx \sum_i f_i(s_{max})^2 \quad (14)$$

The electron radial distribution function (ERDF) analysis for the liquid structure determination by Nishikawa and Iijima[29] was applied to the adsorbed CCl_4 molecular assembly in the micropore. The ERDF $4\pi r^2(\rho(r) - \rho_0)$ is obtained by the Fourier transformation of the structure function, $si(s)$. Here $\rho(r)$ and ρ_0 are the density at a distance r and the average density, respectively.

$$si(s) = s\cdot\{I^{CCl_4}_{coh}(s) - \sum_i f_i(s)^2\} \quad (15)$$

$$4\pi r^2(\rho(r) - \rho_0) = \frac{2r}{\pi\sum Z_j^2}\sum_s si(s)\cdot\sin(sr)\cdot\Delta s \quad (16)$$

where Z_j is the electron number of a component atom j. The ERDF expresses the distribution of the electron clouds.

TABLE 1: Pore Structure of ACF Samples by N_2 Adsorption at 77 K

	micropore volume ($W_0(N_2)$/mL·g^{-1})	surface area (a_α/m^2·g^{-1})	external surface area ($a_{\alpha,ext}$/m^2·g^{-1})	pore width ({$W_0/(a_\alpha/2)$}/nm)
P-5	0.336	900	5	0.75
P-10	0.622	1510	25	0.82
P-20	0.971	1770	44	1.13

Results and Discussion

Micropore Filling of CCl_4. N_2 adsorption isotherms at 77 K were of type I. The specific surface areas a_α, the external surface area $a_{\alpha,ext}$, and the micropore volume $W_0(N_2)$ determined by the subtracting pore effect method using the high-resolution α_s-plots[32] are shown in Table 1. $a_{\alpha,ext}$ is negligibly small compared with a_α. The average pore widths w from both of a_α and $W_0(N_2)$ are also shown in Table 1. The average pore widths of P-5, P-10, and P-20 correspond to the 1.28, 1.33, and 1.92 adsorbed layers, respectively. Here the micropore volume was obtained by use of the bulk N_2 liquid density of at 77 K ($\rho_{N_2} = 0.808$ g·mL^{-1}).

The adsorption isotherms of CCl_4 on ACF at 303 K are shown in Figure 3. They are also of type I. The steeper the initial uptake, the smaller the pore width. All adsorption isotherms reach almost to the plateau above $P/P_0 = 0.2$. Therefore, almost all molecules of CCl_4 are filled in micropores, and the amount of adsorption on the external surfaces can be neglected even under the saturated conditions ($P/P_0 = 1$). The CCl_4 adsorption isotherms were analyzed by the Dubinin−Radushkevich (DR) equation[33]

$$W = W_0^{DR}\cdot\exp\left[-\left(\frac{A}{\beta E_0}\right)^2\right],\quad A = RT\ln(P_0/P) \quad (17)$$

where W is the amount of gas adsorbed at P/P_0 and W_0^{DR} is the micropore volume. The notation β is an affinity coefficient, and E_0 is the characteristic adsorption energy that is associated with the isosteric heat of adsorption $q_{st,\phi=1/e}$ at the fractional filling ϕ of $1/e$, as given by

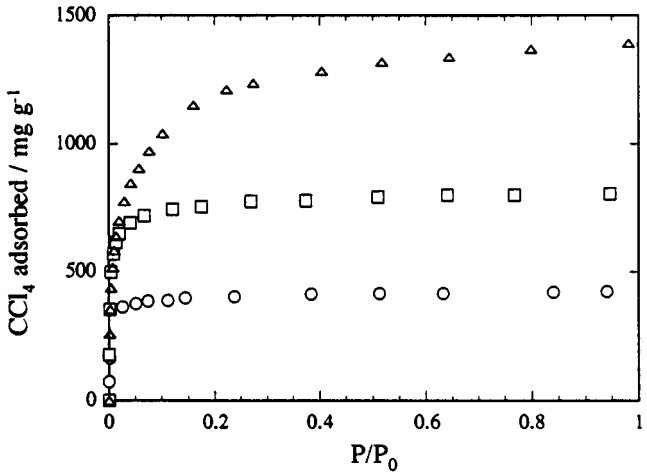

Figure 3. Adsorption isotherms of CCl_4 on ACF samples at 303 K. ○, P-5; □, P-10; △, P-20.

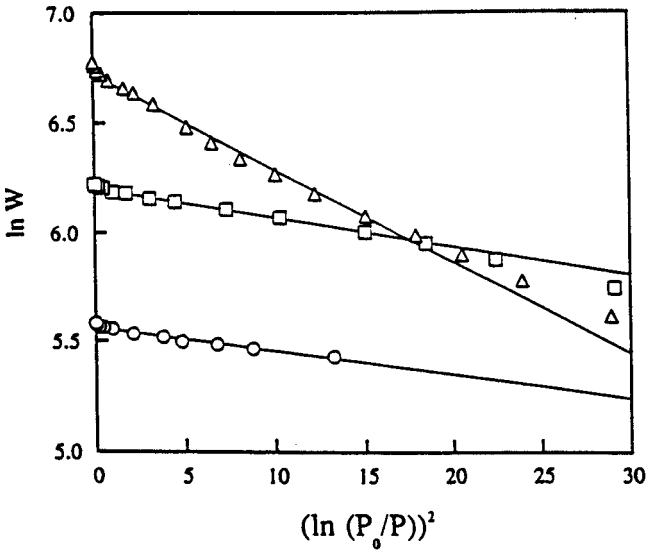

Figure 4. DR-plots of CCl_4 adsorption isotherms at 303 K. ○, P-5; □, P-10; △, P-20.

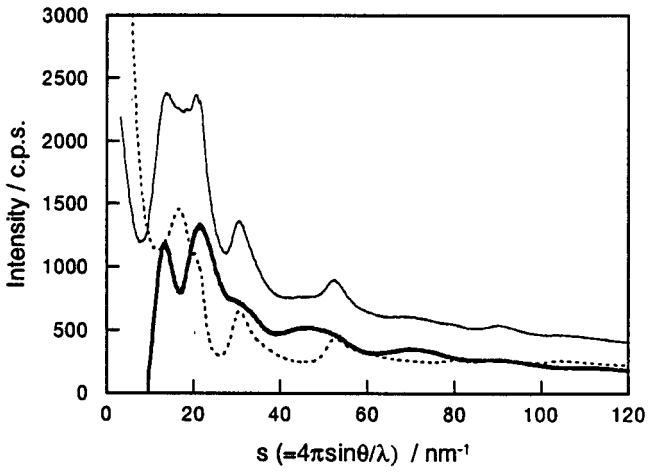

Figure 5. X-ray scattering intensity (arbitrary unit) of P-5 with adsorbed CCl_4. Broken line: the X-ray scattering intensity from the carbon, $I_{tot}^{C}(s)$. Solid line: the X-ray scattering intensity from the CCl_4 adsorbed sample, $I_{tot}(s)$. Bold solid line: the difference of these intensities, $(I_{tot} - I_{tot}^{C})$.

Here ΔH_v is the enthalpy change of vaporization ($\Delta H_v(CCl_4) = 30.0$ kJ·mol^{-1}). Figure 4 shows the DR plots of the CCl_4 adsorption isotherms. These DR plots are linear in the whole range. The micropore volume and $q_{st=1/e}$ for CCl_4 were determined from the DR plots, as shown in Table 2. The $q_{st,\phi=1/e}$ value becomes greater with the decrease of the pore width. The ratio of the average pore width w to the Lennard-Jones parameter σ for CCl_4 is also shown in Table 2. The w/σ values are in the range of 1.3−1.9, and thereby the interaction energy of a CCl_4 molecule with the micrographitic wall strongly depends on the pore width in this range. Hence the observed enhancement in the enthalpy change of adsorption is quite plausible. The micropore volume from CCl_4 adsorption $W_0^{DR}(CCl_4)$ was obtained using the density of bulk liquid CCl_4 at 303 K ($\rho_{CCl_4} = 1.594$ g·mL^{-1}). As the molecular size of CCl_4 is almost two times greater than that of N_2, the intermolecular voids are more predominant with the decrease of the pore width. Therefore, the $W_0^{DR}(CCl_4)/W_0(N_2)$ is much lower than 1; the negative deviation from unity suggests an intense restriction for the molecular packing.

$$q_{st,\phi=1/e} = \beta E_0 + \Delta H_v \qquad (18)$$

X-ray Diffraction of CCl_4 Molecular Assembly. The X-ray diffraction data were corrected by the method mentioned above. I_{tot}^{C} of P-5 and I_{tot} of the CCl_4-adsorbed P-5 are shown in Figure 5 together with $I_{tot} - I_{tot}^{C}$. The difference diffraction intensity $I_{too} - I_{tot}^{C}$, which is assigned to the adsorbed CCl_4, has a similar feature to the bulk CCl_4 liquid. Thus determined X-ray diffraction patterns of the CCl_4 adsorbed in the micropore are shown in Figure 6 as a function of the pore width. All patterns of Figure 6 have the strong first peak (A) and the second peak (B) at 16 and 21 nm^{-1}, respectively. Their positions fairly coincide with those of the bulk liquid CCl_4. However a distinct difference is observed in the intensity ratio of the first and second peaks. The intensity of the first peak (A) decreases with the decrease of the pore width, suggesting an apparent restriction effect for the CCl_4 molecular packing. The marked intensity decrease of the first peak (A) indicates an imperfect long range order. The ERDF analysis provides a clear physical insight, as described below.

Organized Structure of CCl_4 Molecules in a Graphitic Nanospace. Figure 7 shows the ERDF of bulk liquid CCl_4 at 303 K. The ERDF function within 1.5 nm agrees well with the published data on liquid CCl_4 with an energy-dispersive X-ray diffractometer.[34] The peaks of E at 1.1 nm, G at 1.55 nm, and H at 2.0 nm are attributed to the second, third, and fourth-neighbor molecules, respectively. We cannot measure precisely the scattering intensities in the s region smaller than 7 nm^{-1}, and thereby no perfect coincidence above 2 nm was obtained. Hence, we must be careful in the discussion of the radial distribution function over the 2.0 nm range in this work.

Figure 8 shows the ERDF of CCl_4 adsorbed in the micropores at 303 K and $P/P_0 = 1$. The D and E peaks are ascribed to the first- and second-nearest-neighbors, respectively. Both the D and E peaks are sensitively affected by the micropore size. Figure 9 compares the peak position and intensity of both the D and E peaks. The position of peak D is independent of the pore width, being the same as that of bulk liquid. On the other hand, the position of peak E shifts to the shorter position with the decrease of the pore width. The peak intensity of both D and E decreases with the decrease of the pore width. These results suggest the presence of the intense restriction of CCl_4 molecular packing in the narrower micropore; the serious restriction in the narrower micropore should prohibit the bcc structure[29] of the bulk CCl_4 liquid and reduce the number of the first-nearest and second-nearest-neighbor molecules. That is, the predominant restriction for packing of CCl_4 molecules gives rise to defects in the nearest-neighbor coordination,

TABLE 2: Comparison of the N_2 and CCl_4 Adsorbed Volume of ACFs

	isosteric heat of adsorption ($q_{st,\theta=1/e}$/kJ·mol^{-1})	micropore volume ($W_0^{DR}(CCl_4)$/mL·g^{-1})	pore volume ratio ($W_0^{DR}(CCl_4)/W_0(N_2)$)	ratio of pore width to molecular diameter (w/σ)
P-5	54.3	0.260	0.77	1.3
P-10	46.9	0.495	0.80	1.4
P-20	42.2	0.826	0.85	1.9

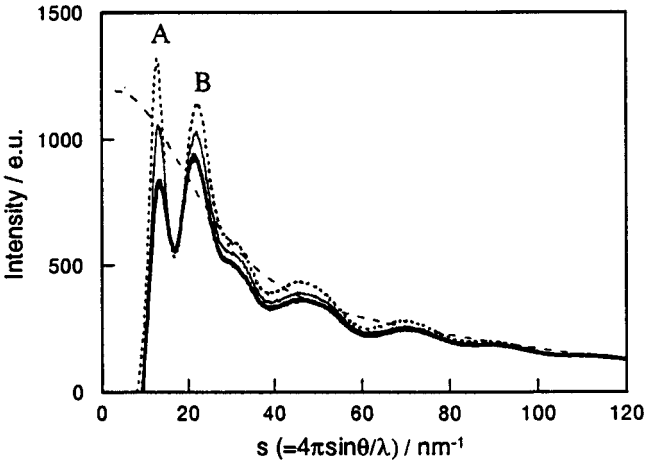

Figure 6. X-ray scattering intensities (in electron units) of CCl_4 adsorbed in the micropores of three kinds of ACFs at 303 K. Bold line: $w = 0.75$ nm (P-5). Solid line: $w = 0.82$ nm (P-10). Broken line: $w = 1.13$ nm (P-20).

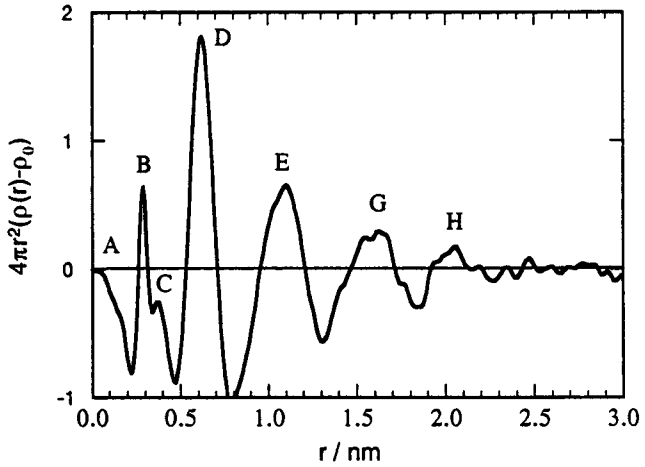

Figure 7. Radial distribution function of the bulk liquid CCl_4 at 303 K.

accompanying with the remarkable change in the second-neighbor coordination. Then, the peak D does not shift, while the peak E shifts to the shorter side.

Furthermore, a distinct difference between the adsorbed CCl_4 and the bulk liquid is observed in the range of 1.0−2.0 nm. The intensity of E, G, and H peaks decreases with the pore width, indicating that the organized CCl_4 assemblies are limited within the fourth-neighbor coordination at best. This should be also associated with the fact that the molecular assemblies are restricted in the two-dimensional space. Therefore, the intensity due to the second−fourth-neighbor coordination becomes much smaller than that of the bulk liquid.

CCl_4 molecules adsorbed in the narrowest pore of P-5 have a new peak (F) at 1.33 nm in Figure 8, suggesting the presence of a characteristic molecular arrangement different from the bulk liquid structure. The presence of this new peak was suggested in the course of the molecular simulation study by the grand canonical Monte Carlo method.[35] The specific structure different from that of bulk liquid should stem from an imperfect packing of CCl_4 molecules in the narrow slit space.

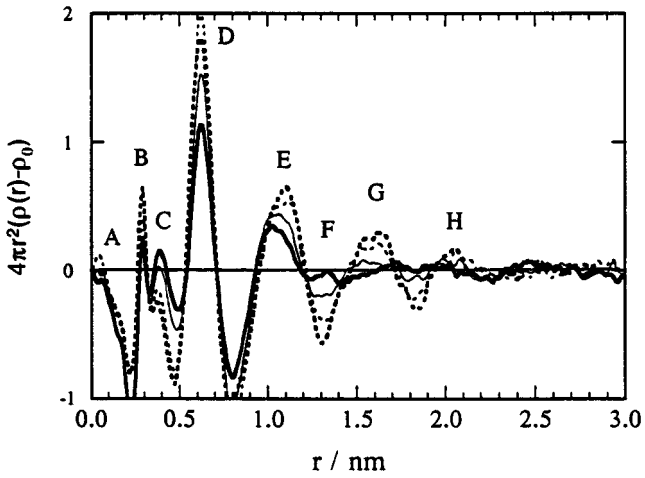

Figure 8. Radial distribution functions of CCl_4 adsorbed in micropores and bulk liquid CCl_4 at 303 K. Bold line: $w = 0.75$ nm (P-5). Solid line: $w = 0.82$ nm (P-10). Broken line: $w = 1.13$ nm (P-20). Bold broken line: bulk liquid.

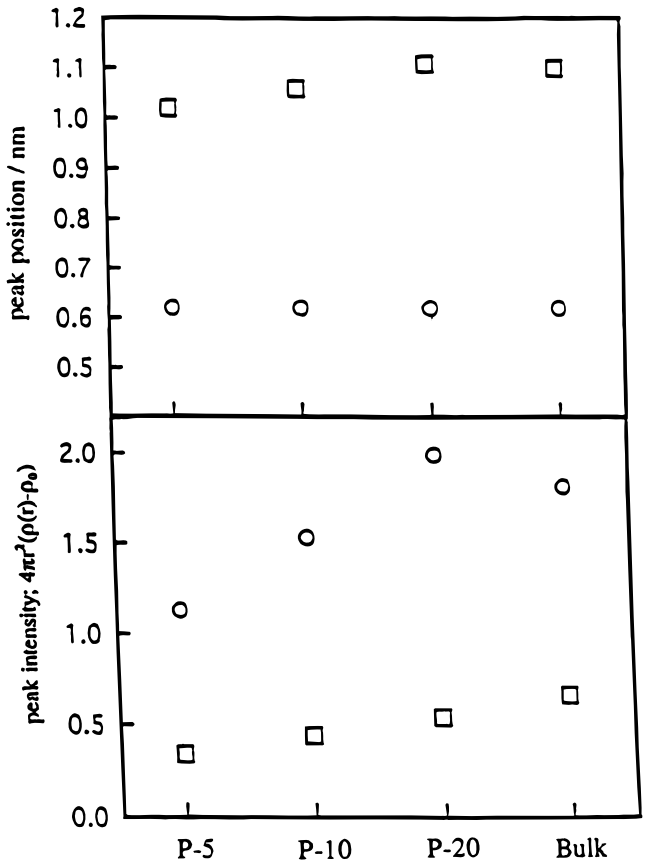

Figure 9. Changes in the peak position and intensity of the first-nearest-neighbor and second-nearest-neighbor peaks. (○), the first-neighbor peak (D); □, the second-neighbor peak (E).

The shoulder A and the peak B at 0.18 and 0.29 nm, respectively, in Figure 8 are attributed to the C−Cl and Cl−Cl intramolecular atomic correlations, respectively. The peak of bulk liquid (C) at 0.38 nm is assigned to the intermolecular Cl−Cl atomic correlation for the first-nearest-neighbor mol-

ecules. Only the intensities of the peak C increase with the decrease of the pore width. This peak should include the scattering due to the CCl_4−carbon interface correlation because the contact distance of CCl_4 molecule with the surface carbon atom is close to the intermolecular Cl−Cl distance. The contact becomes predominant in narrower pores, increasing the intensity of peak C. So far the absolute value of adsorbed CCl_4 density ρ_0 cannot be directly determined from these X-ray diffraction measurements. However, this paper describes the effectiveness of the ERDF analysis using the density difference $(\rho(r) - \rho_0)$ for X-ray diffraction to determine the molecular assembly confined in the micropore.

Acknowledgment. We acknowledge the Ministry of Education for the Grant-in-Aid for Scientific Research on Priority Areas (Carbon Alloys) of Japanese Government. T.I. is supported by Research Fellowship of Japan Society for the Promotion of Science for Young Scientists.

References and Notes

(1) Everett, D. H.; Powl, J. C. *J. Chem. Soc., Faraday Trans.* **1976**, *72*, 619.
(2) Cracknell, R. F.; Gubbins, K. E.; Maddox, M.; Nicholson, A. *Acc. Chem. Res.* **1995**, *28*, 281.
(3) Imai, J.; Souma, M.; Ozeki, S.; Suzuki, T.; Kaneko, K. *J. Phys. Chem.* **1991**, *95*, 9955.
(4) Kaneko, K.; Shimizu, K.; Suzuki, T. *J. Chem. Phys.* **1992**, *97*, 8705.
(5) Kaneko, K.; Fukuzaki, N.; Ozeki, S. *J. Chem. Phys.* **1987**, *87*, 776.
(6) Kaneko, K.; Fukuzaki, N.; Suzuki, T.; Kakei, K.; Ozeki, S. *Langmuir* **1989**, *5*, 960.
(7) Kanoh, H.; Kaneko, K. *J. Phys. Chem.* **1996**, *100*, 755.
(8) Wang, Z. W.; Kaneko, K. *J. Phys. Chem.* **1995**, *99*, 16714.
(9) Fujie, K.; Minagawa, S.; Suzuki, T.; Kaneko, K. *Chem. Phys. Lett.* **1995**, *236*, 427.
(10) Bonardet, J.; Fraissard, J.; Unger, K.; Diptka, K.; Ferrero, M.; Ragle, J.; Cunnar, W. C. *Characterization of Porous Solids III*; Elsevier Science Publishing: New York, 1994; Vol. 87, p 319.
(11) Imai, J.; Kaneko, K. *Langmuir* **1992**, *8*, 1695.
(12) Patrick, J. W. *Porosity in Carbons*; Edward Arnold: London, 1995.
(13) Bansal, R. C.; Donnett, J. B.; Stoeckli, F. *Active Carbons*; Marcel Dekker: New York, 1988.
(14) Fung, A. W. P.; Dresselhous, M. S.; Endo, M. *Phys. Rev.* **1993**, *B48*, 14953.
(15) Ishii, C.; Matsumura, Y.; Kaneko, K. *J. Phys. Chem.* **1995**, *99*, 5744.
(16) Ruike, M.; Kasu, T.; Setoyama, N.; Suzuki, T.; Kaneko, K. *J. Phys. Chem.* **1995**, *99*, 9594.
(17) Nakayama, A.; Suzuki, K.; Enoki, T.; Ishii, C.; Kaneko, K.; Endo, M.; Shindo, N. *Solid State Commun.* **1995**, *34*, 323.
(18) Kaneko, K.; Ishii, C.; Ruike, M.; Kuwabara, H. *Carbon* **1992**, *30*, 1075.
(19) Setoyama, N.; Ruike, M.; Kasu, T.; Suzuki, T.; Kaneko, K. *Langmuir* **1993**, *9*, 2612.
(20) Setoyama, N.; Kaneko, K.; Rodriguez-Reinoso, F. *J. Phys. Chem.* **1996**, *100*, 10331.
(21) Kaneko, K.; Kosugi, N.; Kuroda, H. *J. Chem. Soc., Faraday Trans. 1* **1989**, *85*, 869.
(22) Seaton, N. A.; Walton, J. P. R. B.; Quirke, N. *Carbon* **1989**, *27*, 853.
(23) Cracknell, R. F.; Nicholson, D. *J. Chem. Soc., Faraday Trans.* **1994**, *90*, 1487.
(24) Muller, E. A.; Rull, L. F.; Vega, L. F.; Gubbins, K. E. *J. Phys. Chem.* **1996**, *100*, 1189.
(25) Iyama, T.; Nishikawa, K.; Otowa, T.; Kaneko, K. *J. Phys. Chem.* **1995**, *99*, 10075.
(26) Narten, A. H. *J. Chem. Phys.* **1976**, *65*, 373.
(27) Egelstaff, P. A.; Page, D. I.; Powles, J. G. *Mol. Phys.* **1971**, *20*, 881.
(28) Nishikawa, K.; Murata, Y. *Bull. Chem. Soc. Jpn.* **1979**, *52*, 293.
(29) Nishikawa, K.; Iijima, T. *Bull. Chem. Soc. Jpn.* **1985**, *58*, 1215.
(30) MacGillavry, C. H. *International Tables for X-ray Crystallography*; Kluwer Academic Publishers: Dordrecht, 1989; Vol. IV.
(31) Suzuki, T.; Kaneko, K. *Chem. Phys. Lett.* **1992**, *191*, 569.
(32) Kaneko, K.; Ishii, C. *Colloids Surf.* **1992**, *67*, 203.
(33) Dubinin, M. M. *Chemistry and Physics of Carbon*; Marcel Dekker: New York, 1966; Vol. II, p 51.
(34) Murata, Y.; Nishikawa, K. *Bull. Chem. Soc. Jpn.* **1978**, *51*, 411.
(35) Suzuki, T.; Gubbins, K. E.; Kaneko, K. *Langmuir*, in press.